Ultrafast Excited-State Proton Transfer of 2-(2′-Hydroxyphenyl)benzothiazole: Theoretical Analysis of the Skeletal Deformations and the Active Vibrational Modes†

Regina de Vivie-Riedle,‡,§ Vincent De Waele,§,||,⊥ Lukas Kurtz,§ and Eberhard Riedle*,||

Department Chemie, Ludwig-Maximilians-Universität, Butenandt-Str. 11, D-81377 München, Germany, Max-Planck-Institut für Quantenoptik, 85748 Garching, Germany, and Lehrstuhl für BioMolekulare Optik, Sektion Physik, Ludwig-Maximilians-Universität, Oettingenstr. 67, D-80538 München, Germany

Received: May 4, 2003; In Final Form: September 24, 2003

The involvement of skeletal deformations in the ultrafast excited-state proton transfer of 2-(2′-hydroxyphenyl)-benzothiazole (HBT) and the identification of the vibrational modes active in the process are reported. A multidimensional ab initio calculation of ground and excited states at the HF/DFT and CIS/TDDFT level renders the relevant portions of the potential energy surfaces around the minimum-energy path connecting the enol and keto configuration. The frequencies and potential energy distributions of the normal modes and the corresponding deformations of the molecule are calculated for all minimum-energy geometries. Along the minimum-energy path, the nuclear deformation is projected onto the relevant normal modes. This normal-mode analysis shows that mainly five low-frequency in-plane vibrations are associated with the electronic rearrangement and the transfer of the proton. The theoretical findings are in quantitative agreement with the experimental study presented in the accompanying paper.

I. Introduction

The study of excited-state intramolecular proton transfer (ESIPT) has been an active area of research since the first experimental observation of the phenomenon by Weller in the middle of the last century.[1] ESIPT occurs in molecules containing both acidic and basic groups in close proximity that may rearrange in the excited electronic state via a proton or hydrogen atom transfer. The strong and fast reorganization of the charge distribution resulting from the tautomerization makes these molecules very attractive to design and use in fluorescence sensors,[2,3] laser dyes and LEDs,[4,5] UV filters,[6−9] and molecular switches.[10,11]

The relevant processes connected to ESIPT are shown in Figure 1 for the case of 2-(2′-hydroxyphenyl)benzothiazole (HBT). After the optical excitation of the enol conformer, ESIPT occurs, the covalent bond of the proton with the oxygen atom is changed to an intramolecular hydrogen bond, and the original hydrogen bond with the nitrogen atom is changed to a covalent bond. Later, the molecule returns to the electronic ground state by fluorescence or internal conversion. Finally, the proton is transferred back in a thermal process. The emission of the keto tautomer is strongly red shifted from the enol absorption spectrum. This scheme is general for all ESIPT systems, and it is now well established that proton transfer (PT) itself can proceed on the subpicosecond time scale.[12−32] ESIPT proceeds adiabatically on the S_1 hypersurface[12,33−37] whereas the internal conversion (IC) channel is due to a surface crossing or a conical intersection and occurs on varying time scales.[14,22,25,27,30,38] In most cases, the PT and the IC can be considered to be decoupled, as observed in ultrafast pump−probe experiments.[27]

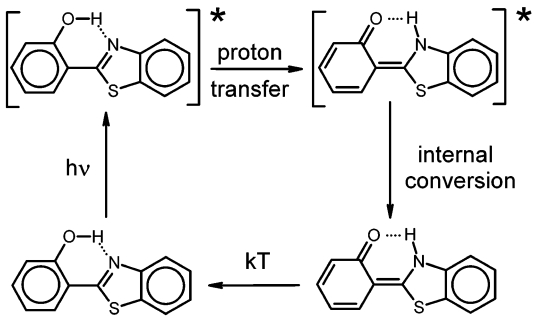

Figure 1. Schematic representation of excited-state proton transfer in HBT. Photoexcitation initiates proton transfer to the excited keto tautomer. After internal conversion, the proton is transferred back.

ESIPTs ultrafast dynamics ($k_{ESIPT} > 10^{12}$ s^{-1}) challenges spectroscopy as well as theory, and it requires an understanding of the interplay between structure, dynamics, and reactivity. The time scale of ESIPT is comparable to the period of the low-frequency molecular modes, and one expects a better understanding of the process by learning about the vibrational dynamics that drive and follow the PT. Until recent advances in the development of tunable sources of ultrashort laser pulses, information concerning ESIPT vibrational dynamics was limited to a few resonance Raman (RR) studies.[39−42] The new developments in time-resolved spectroscopy allow the observation of highly localized wave packets even in large reactive molecular systems in the condensed phase. In particular, ESIPT was studied in two-color pump−probe experiments using 25- to 30-fs pulses that revealed wave packet motions during and following the ESIPT process for several PT systems.[17,23,24,26,27,29,43,44] All of these studies in the time and frequency domain emphasize the participation of low-frequency modes. However, different experiments are sensitive to different

† Part of the special issue "Charles S. Parmenter Festschrift".

* Corresponding author. E-mail: riedle@physik.uni-muenchen.de. Phone: +49-89-2180-9210.

‡ Department Chemie, Ludwig-Maximilians-Universität.

§ Max-Planck-Institut für Quantenoptik.

|| Lehrstuhl für BioMolekulare Optik, Ludwig-Maximilians-Universität.

⊥ Present address: Laboratoire de Chimie Physique, UMR 8000 C.N.R.S. Bat 349, Université Paris-Sud, Orsay, France.

10.1021/jp035204r CCC: $25.00
Published on Web 11/05/2003

locations on the excited-state surface; therefore, the contribution of the modes to the ESIPT process is still not well established. The aim of this work is to investigate theoretically the vibrational dynamics during and after the ESIPT process of HBT and to provide a well-founded interpretation of the experimental observations presented in the accompanying paper.[44]

After the UV excitation of the enol tautomer, the HBT molecule undergoes a fast structural reorganization. In nonpolar solvents or anorganic matrices, this reorganization is characterized by an emission with a Stokes shift of about 8000 cm^{-1}.[13,19] This emission can safely be attributed to a cis planar keto tautomer[45] that is formed within 170 fs.[18] Lochbrunner et al. reported a study of HBT's ESIPT with a time resolution of 30 fs[24,44] and found that the emission signal appears after about 60 fs. The time evolution of the stimulated emission is strongly modulated and consists of four low-frequency vibrational modes with a decay time of about 1 ps.

Recent investigations have shown that the calculation of reliable potential energy surfaces is possible even for the excited electronic states of large reactive molecules.[33−36,46] The energetics and structural parameters of HBT were determined with reasonable accuracy.[45,47] However, no theoretical investigation has been performed that precisely models the ultrafast dynamics and investigates the involvement of skeletal motions in the ESIPT process. To achieve a consistent picture of the complete ESIPT and a detailed microscopic explanation of the ultrafast PT dynamics in HBT, we performed an analysis of the vibrational modes active in the process and compared these to the experimentally observed wave packet motion.[44] A multidimensional ab initio calculation of ground and excited states at the HF/DFT and CIS/TDDFT levels renders the relevant portions of the potential energy surfaces around the minimum-energy path connecting the enol and keto configurations. It allows a discussion of the structural evolution along the minimum-energy path (MEP) and thereby establishes the relation between the observed wave packet dynamics and the ESIPT mechanism.

In section II, the computational methods are summarized. Section III.A investigates all stable molecular structures, their differences, and the associated energies in the ground and excited states. Section III.B extends the structural analysis to the MEPs and determines the two relevant ESIPT coordinates. Section III.C then presents a 2D molecular reaction surface for the ESIPT. In Sections III.D and III.E, we focus all previously collected information to assess the normal modes that drive the ESIPT process and/or are coherently excited by it. This normal-mode information is then related to experimental observations.[44] Finally in section IV a comprehensive model for ESIPT is distilled, and the conclusions are summarized in section V.

II. Computational Methods

In the first step, the electronic structures for the S_0 ground state were computed on the Hartree−Fock (HF) level, and those for the first excited singlet state S_1 were computed on the CIS level, both with the 6-31G* basis. The geometries were optimized, and vibrational force fields were calculated. The energy of the optimized structure was subsequently corrected using the density functional theory (DFT) and time-dependent DFT (TDDFT) method with the B3LYP functional for the ground and excited states, respectively.

We further employed the above-mentioned HF and CIS methods for the proton transfer's MEPs in the ground and excited states and added single-point DFT and TDDFT energy corrections appropriately. The reliability of this approach for the MEP has already been established in detailed ab initio studies and in comparisons with CCSD and CASSCF/PT2 methods for smaller PT systems.[33,34,36,37,46,48]

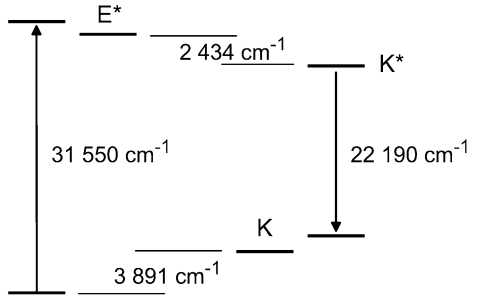

Figure 2. Excitation and fluorescence scheme and energies of the stationary and Franck−Condon structures in HBT. See section III.A.1 and Table 1 for details.

All electronic structure calculations were performed with Gaussian 98.[49] The Hessian of the potential energy was derived for all stable structures, and the frequencies and normal modes were determined from it. Because the normal-mode analysis relies only on the potential shape in close proximity to the equilibrium, it was sufficient to evaluate the vibrational frequencies in the S_1 state at the CIS level. For the S_0 state, we were able to verify explicitly the validity of this approximation by comparing the frequencies calculated with HF and DFT. No significant differences were found. The comparison of the S_1 potential energy surface (PES) around the equilibrium structure showed a nearly unchanged shape at the CIS and TDDFT levels. We therefore conclude that the CIS vibrational frequencies are accurate enough for the analysis of ESIPT.

With the REDONG program,[50] we projected the Cartesian force fields onto a set of redundant internal coordinates. The results were used to calculate the vibrational potential energy distribution. Subsequently, the contribution of the normal modes to the deformation of the molecule along the reaction path was investigated within the formalism of the normal-mode analysis.[51]

III. Results

The ESIPT of HBT is a photoinduced mechanism in which a $\pi\pi^*$ electronic excitation initiates an electronic reorganization that leads to a bond breaking and formation process associated with a structural reorganization of the whole molecule. These processes are intimately linked and result in observed ultrafast reaction times of about 50 fs.[44]

III.A. Structure and Energy of the Stationary Points. *III.A.1. Energy Diagram of the Proton Transfer.* The determination of the equilibrium structures and their differences provides the first ideas of how the molecular frame readjusts while the proton is transferred. Hence, we searched for all stationary molecular geometries in the ground and excited states. HBT was already optimized in the S_0 and S_1 states with the 3-21G* basis set.[45] To avoid any effect of this limited basis set on the calculated structures, we used the larger 6-31G* basis, which is much more appropriate for the description of the vibrational properties and for DFT and TDDFT computations. Moreover, we determined how reliable the optimized structures are by reproducing the energetic scheme inferred from the spectroscopy of HBT.

In the S_0 as well as in the S_1 state, we found two stable minima corresponding to enol- and keto-like configurations. The enol tautomer is the global minimum in the S_0 state whereas the keto tautomer is energetically favored in the S_1 state (Figure 2).

TABLE 1: Calculated Energies of Ground- and Excited-State HBT for the Enol (E) and Keto (K) PES Minima[a]

structure	difference	energy
E		−1028.98764 au[b]
E*		−1028.85370 au[c]
K		−1028.96991 au[b]
K*		−1028.86479 au[c]
	E − K	−0.482 eV / −3891 cm^{-1}
	E* − K*	0.302 eV / 2434 cm^{-1}
E	S_0/S_1	3.912 eV / 31 550 cm^{-1}
K*	S_1/S_0	2.751 eV / 22 190 cm^{-1}

[a] Energy differences are shown for the minima of each electronic state and the vertical transitions from the global minima (Franck−Condon points; lowest two lines). [b] HF/DFT. [c] CIS/TDDFT.

For these equilibrium structures, the TDDFT method was applied to obtain more precise values of the vertical and adiabatic transition energies. The energies calculated for all of the optimized geometries and the relevant energy differences are given in Table 1. There is no structural or vibrational data of the transient states available from experiment, and the level scheme provides the only check, although indirect, of the optimized HF and CIS structures. The HBT ground-state absorption in cyclohexane peaks at 29 700 cm^{-1}, and the maximum of the emission band is red shifted to 18 500 cm^{-1}.[24] For the vertical transitions, we find deviations of only 0.23 and 0.45 eV for the enol and keto forms, respectively.

In the S_0 state, the keto structure (K) lies 3891 cm^{-1} above the enol minimum (E), and the S_1 state sees a 2434-cm^{-1} stabilization of the keto geometry (K*) versus the enol structure (E*). ESIPT processes are characterized by a strongly Stokes shifted 0−0 transition of the keto configuration (emission spectrum) relative to the 0−0 transition of the enol configuration (absorption spectrum). The Stokes shift is given by the sum of the stabilization energies and has been evaluated to be 7500 cm^{-1} for HBT in cyclohexane,[13,44] in reasonable agreement with the calculated value of 6325 cm^{-1}. We conclude that HBT's Stokes shift mainly results from the destabilization of the ground-state keto minimum. This has already been proposed for other ESIPT systems,[15,36] and the partitioning of the Stokes shift agrees with the values measured for the 2-(2′-hydroxyphenyl)benzoxazole (HBO) molecule (4900 and 2100 cm^{-1}).[52] Our results contradict the situation in a low-temperature matrix where a stronger stabilization of the keto S_1 state and a smaller destabilization of the S_0 state[19] were found. Because DFT methods are very reliable for predicting the ground-state properties of aromatic compounds, it can be assumed that the discrepancy is caused by the surrounding low-temperature matrix.

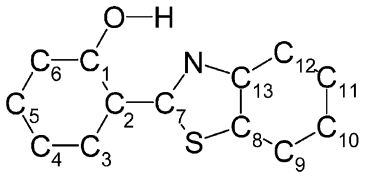

Figure 3. Labeling of the atoms in HBT.

III.A.2. Structural and Electronic Changes Associated with ESIPT. The bond lengths of the optimized geometries of E, E*, K, and K* and the ON distance that is crucial to ESIPT are reported in Table 2. (For atoms labeling, see Figure 3.) The conversion from E to K* is a complex process that intimately links electronic and structural reorganizations. To identify and clarify the rearrangement attributed to PT, we compare the different structures pairwise: E/E*, E*/K*, K/K*, E/K. These pairs correspond to the photoinduced electronic transition, ESIPT itself, fluorescence deexcitation, and back PT.

E/E*. The first insight into the effect of the electronic excitation is provided by analyzing the HOMO and LUMO orbitals represented in Figure 4 for the E and K conformations. Two remarkable features emerge from the enol orbitals (Figure 4a). First, the S_1-S_0 transition affects the π density of the CC bonds constituting the chelate ring. The bonding character along the C_2C_7 inter-ring bond is increased, while the π density on the C_1C_2 and C_7N bonds is reduced. As a consequence, the acidic character of the phenol group and the basic character of the benzothiazole group are altered, and a shortening of the C_2C_7 bond (−0.078 Å) and a lengthening of the C_1C_2 and C_7N bonds (+0.055 and +0.080 Å, respectively) results. In addition to these changes in the H-chelate ring, there are also significant geometric changes in the thiazole ring. The second remarkable signature is the charge-transfer character of the transition. The

TABLE 2: Bond lengths (in Å) for the Optimized Structures of the Ground- (HF/6-31G*) and Excited-State (CIS/6-31G*) HBT in the Enol and Keto Conformations[a]

			E	excitation	E*	ESIPT	K*	fluorescence	K	back PT
C_2C_3	phenol		1.401	0.026	1.427	−0.037	1.390	0.047	1.437	−0.036
C_3C_4	phenol		1.373	−0.005	1.368	0.039	1.407	−0.063	1.344	0.029
C_4C_5	phenol		1.394	0.016	1.410	−0.018	1.392	0.047	1.439	−0.045
C_5C_6	phenol		1.374	0.009	1.383	0.005	1.388	−0.044	1.344	0.030
C_6C_1	phenol		1.395	−0.011	1.384	0.034	1.418	0.037	1.455	−0.060
C_1C_2	phenol	H-chelate	**1.404**	**0.055**	**1.459**	**0.030**	**1.489**	**−0.030**	**1.459**	**−0.055**
C_1O		H-chelate	1.331	0.010	1.341	−0.075	1.266	−0.035	1.231	0.100
OH		H-chelate	0.957	0.014	0.971	0.888	1.859	−0.048	1.811	−0.854
HN		H-chelate	1.867	−0.059	1.808	−0.800	1.008	0.002	1.010	0.857
ON		H-chelate	2.689	−0.056	2.633	−0.008	2.625	−0.033	2.592	0.097
C_2C_7		H-chelate	1.470	−0.078	1.392	0.015	1.407	−0.018	1.389	0.081
C_7N	thiazole	H-chelate	**1.279**	**0.080**	**1.359**	**−0.004**	**1.355**	**−0.021**	**1.334**	**−0.055**
NC_{13}	thiazole		1.384	−0.051	1.333	0.040	1.373	0.011	1.384	0.000
C_7S	thiazole		1.765	0.086	1.851	−0.036	1.815	−0.057	1.758	0.007
SC_8	thiazole		1.746	0.061	1.807	0.013	1.820	−0.058	1.762	−0.016
$C_{13}C_8$	thiazole	benzene	**1.390**	**0.037**	**1.427**	**−0.033**	**1.394**	**−0.008**	**1.386**	**0.004**
C_8C_9		benzene	1.388	−0.011	1.377	0.001	1.378	0.004	1.382	0.006
C_9C_{10}		benzene	1.380	0.010	1.390	−0.020	1.370	0.005	1.375	0.005
$C_{10}C_{11}$		benzene	1.397	0.013	1.410	−0.017	1.393	−0.002	1.391	0.006
$C_{11}C_{12}$		benzene	1.378	−0.010	1.368	0.016	1.384	−0.012	1.372	0.006
$C_{12}C_{13}$		benzene	1.392	0.028	1.420	−0.027	1.393	−0.008	1.385	0.007

[a] For reference, the changes during excitation, proton transfer (ESIPT), fluorescence/IC, and back PT are given.

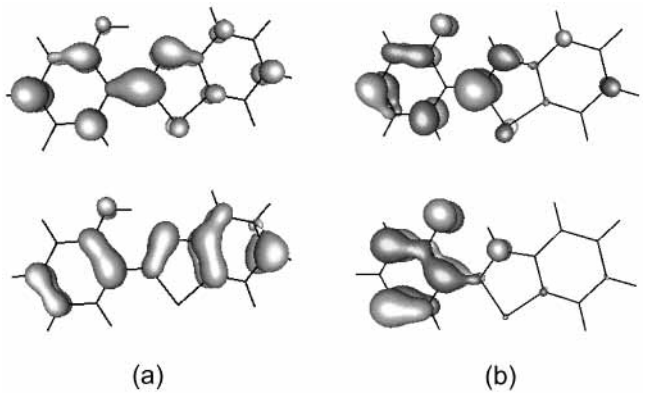

Figure 4. HOMO and LUMO orbitals of (a) enol and (b) keto HBT.

excitation of the electron from the HOMO to the LUMO pushes the electronic density toward the phenol part of the molecule. The changes in the electronic density are advantageous for PT. They modify the charge distribution on the H-chelate ring and thus alter the acidic and basic character of the phenol and benzothiazole groups, respectively.

E*/K*. The OH σ bond is broken, and the NH σ bond formed. This leads to a further rearrangement of the electronic density in the H-chelate ring and a shortening of the C_1O bond (-0.075 Å). But the distortions are not restricted to the H-chelate ring and affect the whole molecule except the benzene ring. The phenol ring loses its aromatic character. The complete reorganization of the molecular skeleton is required to compensate for the electronic changes in the H-chelate ring accompanying the ESIPT.

It is interesting that the structurally different E/E* and E*/K* are mostly opposite in sign, with comparable amplitudes for all of the bonds. This demonstrates that from the FC geometry the molecule can either relax toward the E* local minimum or proceed to the K* global minimum (i.e., ESIPT happens).

K/K*. For the keto conformer, the electronic distribution remains similar in the ground and excited states. The chromophore is localized on the phenol moiety, and the deexcitation induces small changes in the H-chelate ring electronic density (Figure 4b). Accordingly, only comparatively small changes in the bond lengths within the H-chelate ring are found. The phenol and thiazole rings are deformed more strongly.

E/K. For the enol- and the keto-type ground-state minima, large geometrical rearrangements are observed. The OH and NH bonds interchange, and the chelate ring geometry changes (i.e., the C_1O (-0.100 Å) and C_2C_7 bond lengths (-0.081 Å) are shortened, and the C_1C_2 and C_7N bonds are stretched (both $+0.055$ Å)). The large electronic reorganization of the chelate ring is counterbalanced by significant geometrical changes in the phenol ring. The changes between the ground state structures correspond qualitatively to the Lewis formulas represented in Figure 1.

The optical excitation promotes the molecule from the S_0 state to the Franck−Condon (FC) region of the S_1 state. From there, it can either relax to the E* configuration and/or PT can lead to the K* conformer. From the vibrationally relaxed K* conformation, the molecule returns to the electronic ground state with high probability by internal conversion.[44] However, the fluorescence spectrum corresponds to a vertical transition to the keto FC region of the S_0 state.

III.B. Minimum-Energy Path. The MEPs connecting the two stable structures in each electronic state were calculated to identify the major coordinates involved in the PT process. The

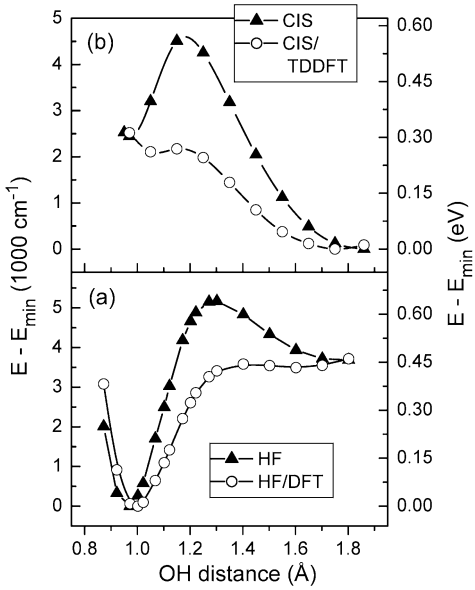

Figure 5. Energy variation along the minimum-energy path from the enol to the keto tautomer of HBT. Calculated for (a) the ground state at the HF and HF/B3LYP levels and (b) the first excited state at the CIS and CIS/TDDFT levels.

results are given in Figure 5a for the ground state and in Figure 5b for the excited state. We utilized the distinguished coordinate approach[33] with the OH bond elongation as the primary reaction coordinate. For the S_0 state, all of the other degrees of freedom were relaxed without imposing any symmetry constraints. This was not possible or even desirable for the S_1 state, and the energies were calculated for the S_0 geometries. The PES is used to describe the ultrafast S_1 dynamics induced by a femtosecond pulse. This situation does not allow for complete relaxation of all modes with respect to the S_0 state, especially not in the FC regime.

In the excited state, the study was restricted to the lowest $^1\pi\pi^*$ excitation. Neither the $^1n\pi^*$ nor the $^1\sigma\pi^*$ state is expected to participate. The $^1n\pi^*$ state could possibly interact with the $^1\pi\pi^*$ state,[35,46] as observed in smaller systems.[53,54] In the case of HBT, the energy stabilization of the $^1n\pi^*$ state is small and lies far above the $^1\pi\pi^*$ state. The $^1\sigma\pi^*$ state should be considered in studies that include nonradiative deactivation to the ground state.[33,38] For HBT, the internal conversion takes place on a time scale of several hundred picoseconds.[14,18] In this study, we are interested in only the much faster ESIPT and can therefore exclude the involevment of the $^1\sigma\pi^*$ state.

The MEP calculations reveal asymmetric curves with one shallow and one deep minimum each, reflecting the enol and keto HBT structures in the ground and $\pi\pi^*$ states. Depending on the electronic configuration, the stability of the minima is exchanged; the enol tautomer is more stable in the ground state, and the keto tautomer is more stable in the excited state. Along both MEPs, the minima are separated by slight barriers whose calculated height strongly depends on the inclusion of electronic correlations.[36,46,47] However, in contrast to smaller molecules,[35] we find from our calculations that electronic correlations do not qualitatively alter the MEPs of HBT. Although slightly shifted, all of the minima remain and have comparable differences in potential energy. We conclude that the CIS method is a suitable approach to study HBT's geometric changes during ESIPT.

Whereas the analysis of the stable configurations (section III.A.2) suggests moderate rearrangements to take place between E* and K*, the MEP analysis finds quite significant skeleton

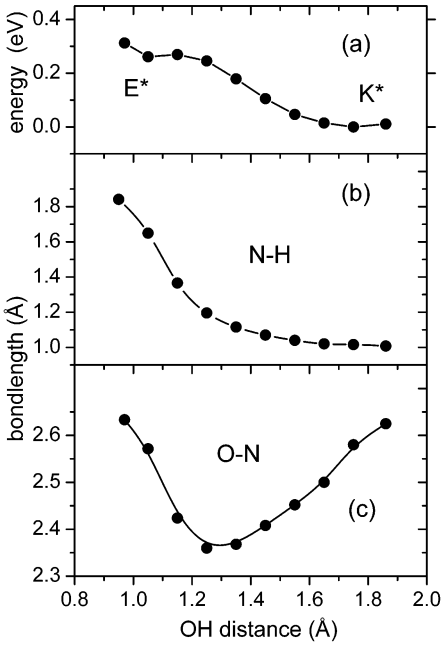

Figure 6. Evolution along the S_1 minimum-energy path of HBT. (a) Energy at the CIS/TDDFT level. (b) NH bond length. (c) ON distance.

distortions during the transfer process. Figure 6 shows the changes in the NH bond length and the ON distance along the MEP as the proton is transferred. The PT is dominated by a large change in the distance between the two heteroatoms. The transfer mechanism can be described in three consecutive phases associated with the three regions (E* minimum, barrier, K* minimum) in the S_1 MEP energetics shown in Figure 6a. In the first phase, the ON distance decreases (from 2.63 to 2.36 Å) along with a shortening of the NH distance (from 1.84 to 1.20 Å), while the OH bond is elongated much less (+0.3 Å). At the barrier, the minimum in the ON distance is reached, and OH bond character is exchanged for NH bond character. Finally, the heteroatoms separate again and the proton remains with the nitrogen.

In the optical excitation, the geometry E is conserved and deviates from E*. The temporal evolution of the S_1 geometry starts from the FC point (with the geometry of E), and when the system passes by the E* geometry, it has already gained considerable momentum. The momentum is sufficient to carry the HBT over the small barrier to K* and thus allows ESIPT. The large gradient of the PES at the FC point is the driving force that initiates ultrafast PT.

III.C. Proton-Transfer Reaction Surfaces. In the MEP analysis, several coordinates were checked for their relevance in describing the PT dynamics. Most of them were found to remain almost constant or to exhibit simple monotonic behavior as a function of the OH distance. Hence, we conclude that the ON and OH distances are best suited to describe the dynamical aspects of proton transfer, and they are used for the computation of a 2D PES. In other words, the 69 vibrational degrees of freedom of HBT are contracted to the 2 relevant reactive coordinates. Such an approach has already been successfully used for the description of the electrocyclic ring opening of cyclohexadiene.[55]

For a meaningful description of the photoinduced ultrafast process, surfaces are needed with large enough areas to include enol- as well as keto-type structures in both electronic states. Most importantly, the FC region must be included; therefore, the relaxation in the 67 dimensions not explicitly considered

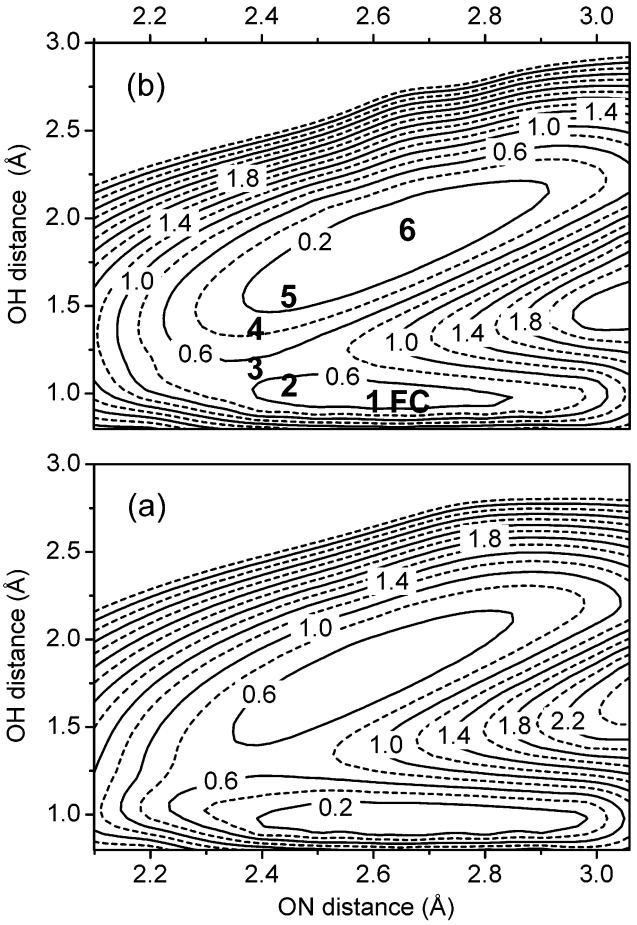

Figure 7. 2D PES of HBT as a function of the ON and OH distances for (a) the ground state and (b) the first excited state. Contour levels are given in eV with respect to the minimum of each state. At the Franck−Condon point (FC) and points 1 to 6 on the reaction path, the NMA was performed. (See section III.E.)

was not allowed on the S_1 surface. First, we calculated a fully relaxed ground-state PES along the OH and ON coordinates at the HF level. For each optimized point (69-dimensional geometry) on the S_0 surface, we then determined the S_1 energy at the CIS level. This procedure enables us to cover the entire area that is relevant to the ESIPT process from the FC region to the excited-state keto minimum.

The S_0 and S_1 PESs along the ON and OH coordinates are shown in Figure 7. The two valleys on both surfaces correspond to the enol and keto conformation. In both cases, the enol form gives rise to a very narrow potential well whereas the keto structure exhibits a wide well. Both conformers are linked by a curved channel bypassing the barrier that hinders direct OH elongation. A representation of the MEP from the FC region to the keto minimum is included as the reaction path (FC and points 1 to 6) in the graph of the S_1 surface.

III.D. Analysis of the Normal Modes. The previous sections dealt with the energetics and the stable structures of the molecular system. Sections III.D and III.E deal with the excited-state normal modes that promote the ESIPT process and accept the excess vibrational energy.

The excited-state normal modes were calculated at the CIS level. We determined for the ground state that the normal modes of HBT are not strongly sensitive to the lack of electronic correlation by comparing HF and DFT results. The confidence we have in CIS relies also on recent detailed experimental and theoretical studies of the vibrational properties of the S_1 state

TABLE 3: Potential Energy Distribution (in %) of the Lowest in Plane Modes of Keto HBT in the S_1 State

vibrational energy (cm^{-1})		
exptl[a]	calcd[b]	potential energy distribution[c]
113	114	$R_{ON}(35)$, $\Delta_{ir}(31)$
255	258	$R_{ON}(22)$, $C_2C_7(16)$.
289	288	$R_{ON}(36)$, $\Delta_{ir}(19)$
	370	$S_{ring}(51)$, $\Delta_{ir}(14)$.
	481	$S_{ring}(66)$.
528	514	$\delta_{CO}(36)$, $S_{ring}(15)$, $R_{ON}(7)$
	534	$Ph_{ring}(25)$, $\delta_{CO}(17)$, $R_{ON}(6)$
	566	$Ph_{ring}(30)$
	630	ring def

[a] Wave packet motion from ref 48. [b] Frequencies CIS/6-31G* scaled by 0.9. [c] Notation for the internal coordinates and PED description. R_{ON}: ON distance. C_2C_7: C_2C_7 bond length. Δ_{ir}: in-plane ring bending. S_{ring}: sulfur ring in-plane deformation. δ_{CO}: in-plane CO bending. Ph_{ring}: in-plane phenol ring deformation. ring def: delocalized in-plane deformation of HBT.

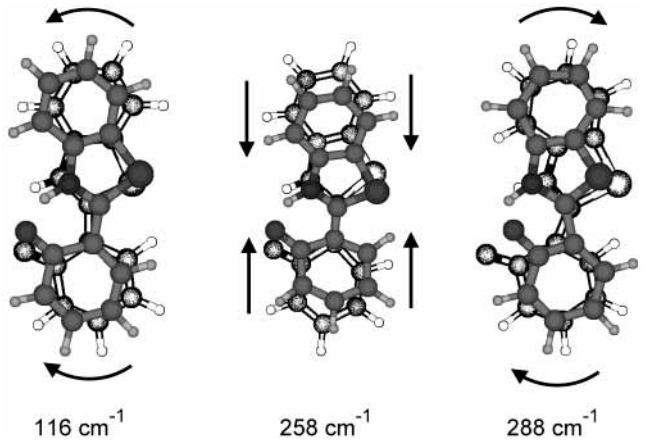

Figure 8. Normal modes of the S_1 keto HBT.

of biphenyl-like molecules whose size and normal modes are comparable to those of HBT.[56,57]

We chose a complete set of internal natural coordinates including the ON distance and calculated the potential energy distribution (PED) of the excited-state keto normal modes.[50] PED determines the contribution of a selected internal coordinate to the potential energy of a normal mode. It allows the determination of the coordinates contributing significantly to a given normal mode. Conversely, the PED of all modes shows which normal modes contribute to the geometric changes associated with ESIPT.

The PED for all low-frequency in-plane modes of the S_1 keto tautomer is reported in Table 3. Only the main contributions to each mode are given. For clarity, we show only the cumulative contribution that affects a specific molecular motion such as the bending of the phenol and benzothiazole groups (called Δ_{ir}, see Table 3 for details regarding notation).

Out of all in-plane modes, only five low-frequency modes are able to modulate the ON distance. PED shows that for three of them this is a dominant contribution (22 to 36%). Two of them are bending modes, and one is a stretching mode of the C_2C_7 inter-ring bond (Figure 8). All frequencies agree closely with those detected in the coherent experimental signal,[24,44] and the occurrence of these five modes demonstrates the multidimensional character of the chelate ring contraction that determines the ESIPT of HBT.

III.E. Normal-Mode Analysis along the Reaction Path. PED shows that only five normal modes contribute to the modification of the ON distance that plays a crucial role in the

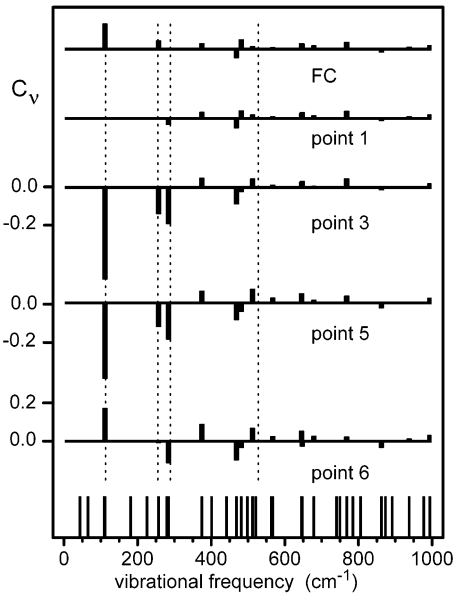

Figure 9. Normal-mode analysis along the minimum-energy path. Shown are the coefficients C_ν for the projection of the molecular deformation from the E* equilibrium geometry onto the E* normal modes. The calculated frequencies are shown as a stick spectrum in the lowest trace. Dashed lines show the experimentally observed frequencies: 113, 255, 289, and 528 cm^{-1}.[44]

ESIPT of HBT. To understand their dynamical interplay and relative significance fully, we investigated the connection between the normal modes and the structural changes along the MEP on the calculated 2D S_1 PES. To this end, a normal-mode analysis (NMA)[51] was performed for several points on the MEP (Figure 7) starting at the FC point close to E*, passing the transition state at point 3, and finally analyzing point 6 in the vicinity of K*.

The deviations of the selected geometries along the MEP from the equilibrium configuration are projected onto the E* and K* normal modes. In other words, we analyze how much of each mode must be added to an equilibrium configuration to result in the molecular structure found at the point of interest.

Combining the positions of all 25 nuclei of HBT in a 75-dimensional vector $\mathbf{X} = (\mathbf{q}_1^T,\mathbf{q}_2^T,...,\mathbf{q}_{25}^T)^T$ and introducing a solution vector $\mathbf{C}$ of equal dimension, we state this analysis as the matrix problem

$$\mathbf{X}_{\text{point i}} - \mathbf{X}_{\text{ref}} = \Theta_{\text{ref}} \cdot \mathbf{C} \qquad (1)$$

For each equilibrium configuration $\mathbf{X}_{\text{ref}}$, the 75×75 matrix Θ_{ref} comprises all 69 vibrational eigenvectors corresponding to the reference configuration as well as the translation of the center of mass and the rotation of the entire molecule to satisfy the Eckart conditions.[51] It is crucial to minimize the influence of relative translation and rotation between $\mathbf{X}_{\text{ref}}$ and $\mathbf{X}_{\text{point i}}$ to ensure solution vector entries C_ν that describe only vibrational contributions. A detailed outline of the method can be found in ref 51.

Because the proton transfer in HBT is an excited-state process, $\mathbf{X}_{\text{ref}}$ is the E* or the K* excited-state equilibrium geometry. Solution coefficients C_ν for $\mathbf{X}_{\text{ref}} = \mathbf{X}_{\text{E*}}$ are displayed in Figure 9; those for $\mathbf{X}_{\text{ref}} = \mathbf{X}_{\text{K*}}$ are given in Figure 10. We will discuss the entire normal-mode frequency range but will restrict the graphical presentation to <1000 cm^{-1} for clarity. From a mathematical point of view, both normal-mode systems are equally appropriate to describe the molecular motion. The

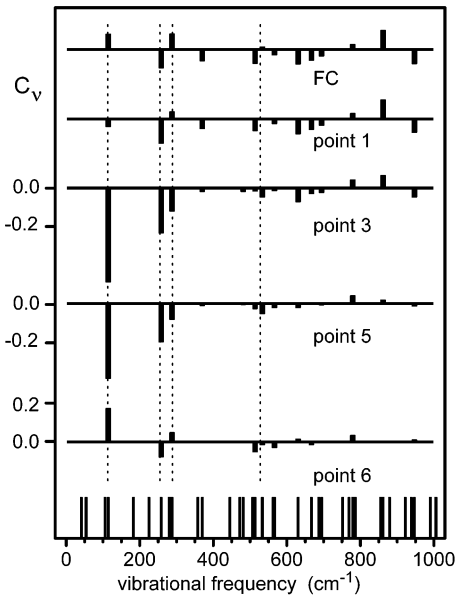

Figure 10. Normal-mode analysis along the minimum-energy path. Shown are the coefficients C_ν for the projection of the molecular deformation from K* equilibrium geometry onto the K* normal modes. The calculated frequencies are shown as a stick spectrum in the lowest trace. Dashed lines show the experimentally observed frequencies: 113, 255, 289, and 528 cm^{-1}.[44]

mode system that suits the situation best has to be selected on physical and/or chemical grounds.

The vibrational frequencies are separated into low- (<1000 cm^{-1}), middle- (1000−1650 cm^{-1}), and high-frequency (>3000 cm^{-1}) regimes. Whereas the low-frequency modes predominantly belong to long-range vibrations involving the entire molecular backbone, modes start to behave increasingly locally with rising frequency. The mid-energy vibrations, for example, deform the benzene ring or the benzothiazole subgroup only, and they also lead to an enhanced motion of the hydrogen atoms attached to the skeleton. The high-frequency modes are restricted to the motion of a few hydrogen atoms. Among them, the highest modes, 3210 cm^{-1} in the E* system and 3266 cm^{-1} for K*, are highly localized in the OH or NH relative motion and do not involve the remaining structure.

At the FC point, the enol configuration is the natural reference. According to Table 2, the ON distance is too large (i.e., the H-chelate ring needs to contract). The 114-cm^{-1} mode is the main contribution to the deformation (see upper panel of Figure 9). As the molecule passes by the E* configuration (point 1), the C_ν all nearly vanish. At point 3, large C_ν's are found corresponding to the strong deformation of HBT. In particular, the three modes at 114, 258, and 288 cm^{-1} dominate. These frequencies agree closely with the experimental values of 113, 255, and 289 cm^{-1}[44] indicated as dashed lines. For the next points on the MEP, the enol reference gives no clear picture except a huge contribution to the phenol OH stretching mode (not shown in the Figures).

At point 3, the electronic configuration changes, and the keto reference (Figure 10) becomes appropriate. Large contributions of the three modes discussed above are again observed and persist even as point 5 is approached. Most of the other modes vanish at points 5 and 6 (i.e., around K*, the 113-, 255-, and 289-cm^{-1} modes are dominant.) In addition, the 514- and 534-cm^{-1} modes are seen, and their sum can be associated with the small contribution found at 528 cm^{-1} in the experiment.[44]

In the enol reference, many of the modes in the 1000−1650-cm^{-1} range show small contributions all along the MEP. In the keto reference, these modes start with quite large C_ν's that diminish around K*. A large contribution to the NH stretch is observed around E* in this reference.

The analysis presented so far is quasi-static. After the optical excitation (i.e., at the FC point), all nuclei are at rest, and the distortion from the E* equilibrium gives rise to significant potential energy. The gradient of the PES points in the direction of the MEP, and the molecule starts to deform accordingly. From the upper panel of Figure 9, we can conclude that the 114-cm^{-1} mode (in-plane bending of the whole molecule) is initially dominating and a contraction of the H-chelate ring results. At point 3, the other four modes with ON distortion start contributing, and eventually the sign of the C_ν's changes in the vicinity of K*. The potential energy is transformed into momentum, and the molecule starts ringing in these activated modes.

IV. Discussion of the ESIPT Mechanism

The results presented in section III give a precise picture of the energetics, the structural and electronic changes, and the MEP of ESIPT in HBT. In addition, a 2D PES and the relevant vibrational modes were presented. On this basis, we now want to discuss the ESIPT mechanism and compare our results to the experimental observations.[44]

Three stable conformations are involved in the ESIPT of HBT: The enol ground-state E and the enol and keto excited states (E* and K*). There is a small barrier along the S_1 MEP that is overestimated at the CIS level but is confirmed even after TDDFT corrections (Figure 5). The 1D MEP alone is not sufficient to describe the PT mechanism. In a multidimensional picture, there is a large barrier between the FC point and the keto minimum. To circumvent this barrier, the molecules first contract the H-chelate ring, and the ON distance is shortened. A region of the PES is reached where only a small barrier has to be overcome for the elongation of the OH bond that leads to the PT. This barrier is identical to the one found for the MEP. At the saddle point, the enol domain of the PES is left, and the keto domain is entered. A similar modulation of the barrier for ESIPT by a variation of the ON distance has also been found for 2-(2′hydroxyphenyl)oxazole.[58] Even for intermolecular PT there is now evidence that low-frequency solvent coordinates control the process.[59,60]

In the static picure of the MEP, the crossing of the barrier cannot be explained. However, in a dynamic picture, the wave packet created at the FC point gains sufficient momentum along the ON coordinate to pass the barrier and evolves into the keto conformation. Because of the topology of the K* minimum, the wave packet now possesses momentum in multiple coordinates, and a back reaction becomes impossible. From the experiment, it is known that HBT's ESIPT proceeds on the 50-fs time scale.[24,44] On this time scale, there has to be a strong coupling between the PT dynamics and the molecular vibrations. Such a coupling was previously discussed for the ground-state PT of phthalic acid monomethylester.[61] Our vibrational analysis demonstrates that only five normal modes are able to modulate the ON distance. The lowest-frequency mode (114 cm^{-1}) is active from the very beginning, and excitation in the other four modes is provided by the barrier crossing and the associated change in electronic configuration.

The actual path of the wave packet will not be identical to the MEP. However, the reaction path will closely follow the MEP because of the tightness of the PES in the enol domain. Therefore, we can safely assume that our analysis of the MEP gives a good approximation of the actual reaction. The geometric analysis presented in the NMA should be closely related to the

temporal evolution of the normal-mode composition of the wave packet. Even though the vibrational and electronic degrees of freedom are tightly linked in the initial phase of ESIPT, the HBT will freely vibrate in the keto modes once it has reached the region of K*. This ringing of the molecule is seen in the ultrafast experiment as oscillatory signal contributions.[44]

The close match between the observed vibrational frequencies of 113, 255, 289, and 528 cm^{-1} and the calculated frequencies of 114, 258, 288, and 514/534 cm^{-1} gives strong support to this model. The lowest-frequency vibration was also recently found to couple to the OD stretching mode in deuterated HBT.[62] In addition, it is reported to couple to the CO mode of K* after a delay of 50 fs,[43] which is exactly the time found for PT in the accompanying experimental work.[44]

It is interesting to compare our present results with the extensive resonance Raman (RR) analysis of the HBT proton-transfer mechanism.[40,41] In this work, the in-plane inter-ring bending mode (293 cm^{-1} in the S_0 state, 288 cm^{-1} in the S_1 state) was identified as the transfer-promoting mode (TPM). The interpretation was based on the overtone progression that reflects a strong anharmonicity in this mode. The RR intensity is related to the propagation of the excited-state wave packet and the Franck−Condon overlap back to the ground state. For a multidimensional PES, the excited-state wave packet quickly leaves the FC region without recurrence. Therefore, RR spectra mainly contain information about the PES around the FC region, sometimes called the "short-time effect" of the Raman intensity. In refs 40 and 41, a dephasing time of 15 fs was concluded, which corresponds to the limiting time during which RR probes the wave packet dynamics. This time is much shorter than the PT time of about 50 fs measured in the time-resolved experiments, and we suppose that for HBT the RR intensities are sensitive only to the PES features in the vicinity of the FC region. The RR observation can be related directly to the reactive process only if there is already a unique reaction coordinate starting in the FC region.

From our analysis and in agreement with the experimental findings, we assign the 114-cm^{-1} bending mode to be the TPM of HBT. We emphasize that this assignment is further supported by the studies on 2-(2′hydroxyphenyl)benzooxazole (HBO) and 2,5-bis(2′benzooxazolyl)hydroquinone,[16,17,63] whose PT units are very similar to those of the HBT molecule. In these experiments, the authors probed the wave packet dynamics prior to the actual ESIPT step and identified the 118-cm^{-1} bending mode of the HBO unit as the TPM.

The five low-frequency in-plane modes associated with the PT in HBT act as accepting modes. Wave packet motion in the analogous transfer-promoting and transfer-accepting modes has also been observed for TINUVIN P,[23] *o*-hydroxybenzaldehyde,[27] and 1-hydroxy-2-acetonaphthone.[26] The presented ESIPT mechanism is completely confirmed in all of these cases.

V. Conclusions

The ESIPT model derived from the ab initio calculations and the normal-mode analysis along the minimum-energy path agrees very well with the considerations derived from the femtosecond pump−probe experiments.[24,44] From the experiments, very precise information can be gathered about the ringing of the molecule after proton transfer in a small number of normal modes. The electronic changes induced by the UV excitation and the initial gradients of the PES (i.e., the driving force responsible for the reactive process) can be clarified only by the calculations.

The optical excitation leads to an electronic density that is intermediate between that of the ground-state enol configuration and that of the excited-state keto configuration. The FC point and the S_1 enol minimum both lie in a potential well that is very narrow along the OH coordinate and shallow along the ON distance. A large barrier therefore exists for the direct PT, and instead a contraction of the ON distance is the initial deformation of HBT. This ON contraction lowers the barrier along the OH coordinate as well as the frequency of the OH vibration[45,47] such that it can mix with low-frequency modes. The channel for PT is finally opened, and the electronic configuration is changed to the keto type. Subsequently, the molecule evolves into the keto well, and five in-plane modes with large changes in the ON distance are coherently excited. The back reaction is hindered because of the multidimensionality of the process and the topology of the PES.

The proton itself does not play an active role, and the OH vibration (before PT) or the NH vibration (after PT) is not excited. Instead, the contraction of the H-chelate ring leads to a shortening of the donor−acceptor distance, and it is this nuclear motion that dominates the initial phase of ESIPT. The 118-cm^{-1} normal mode closely correlates with this contraction, and the mode therefore acts as a promoting mode. After the electronic configuration changes due to UV excitation and PT are complete, the molecule is solely under the influence of the excited-state keto PES and rings freely in the five normal modes connected to the H-chelate ring contraction.

The calculations presented for the ESIPT of HBT reveal a fundamental reaction mechanism that is most likely the basis of the ESIPT of many other molecules with a H-chelate ring as the site of PT. There are even hopes that a full understanding of the ESIPT mechanism will allow the coherent control of the process.[64] We furthermore expect that similar ab initio calculations of chemically reactive systems will elucidate the initial forces that drive the reaction. This analysis is made possible by the identification of a small number of vibrational coordinates out of the $3N - 6$ normal modes closely connected to the deformation of the molecular skeleton caused by electronic excitation. It is this difference between the Franck−Condon geometry reached by the optical excitation and the excited-state equilibrium that drives the reaction. The shape of the PES will then determine the interplay between the various vibrational modes, and quite likely a coherent excitation of selected modes results from the subsequent changes in the electronic configuration. This coherent excitation can then be observed in ultrafast pump−probe experiments as wave packet oscillations. The analysis of the experimental signal will in turn allow the thorough validation of the theoretical predictions.

Acknowledgment. We acknowledge financial support from the Deutsche Forschungsgemeinschaft and the Fonds der Chemischen Industrie. Discussions with S. Lochbrunner and A. J. Wurzer were most helpful.

References and Notes

(1) Weller, A. Z. Z. *Elektrochem*. **1956**, *60*, 1144.
(2) Sytnik, A.; Kasha, M. *Proc. Natl. Acad. Sci. U.S.A.* **1994**, *91*, 8627.
(3) Kubo, Y.; Maeda, S.; Tokita, S.; Kubo, M. *Nature* **1996**, *382*, 522.
(4) Chou, P. T.; Martinez, M. L.; Cooper, W. C.; Chang, C. P. *Appl. Spectrosc.* **1994**, *48*, 604.
(5) Ma, D. G.; Liang, F. S.; Wang, L. X.; Lee, S. T.; Hung, L. S. *Chem. Phys. Lett.* **2002**, *358*, 24.
(6) Chou, P. T.; Studer, S. L.; Martinez, M. L. *Appl. Spectrosc.* **1991**, *45*, 513.
(7) Catalan, J.; Delvalle, J. C.; Fabero, F.; Garcia, N. A. *Photochem. Photobiol.* **1995**, *61*, 118.
(8) Chou, P. T.; Martinez, M. L.; Studer, S. L. *Appl. Spectrosc.* **1991**, *45*, 918.

(9) Keck, J.; Kramer, H. E. A.; Port, H.; Hirsch, T.; Fischer, P.; Rytz, G. *J. Phys. Chem.* **1996**, *100*, 144468.
(10) *Molecular Switches*; Feringa, B. L., Ed.; Wiley-VCH: Weinhein, Germany, 2001.
(11) Photochromism: Memories and Switches; special issue of *Chem. Rev.* **2000**, *100*.
(12) Douhal, A.; Lahmani, F.; Zewail, A. H. *Chem. Phys.* **1996**, *207*, 477.
(13) Ding, K.; Courtney, S. J.; Strandjord, A. J.; Flom, S.; Friedrich, D.; Barbara, P. F. *J. Phys. Chem.* **1983**, *87*, 1184.
(14) Barbara, P. F.; Brus, L. E.; Rentzepis, R. P. M. *J. Am. Chem. Soc* **1980**, *102*, 5631.
(15) Barbara, P. F.; Walsh, P. K.; Brus, L. E. *J. Phys. Chem.* **1989**, *93*, 29.
(16) Arthen-Engeland, Th.; Bultmann, T.; Ernsting, N. P.; Rodriguez, M. A.; Thiel, W. *Chem. Phys.* **1992**, *163*, 43.
(17) Ernsting, N. P.; Kovalenko, S. A.; Senyushkina, T.; Saam, J.; Farztdinov, V. *J. Phys. Chem. A.* **2001**, *105*, 3443.
(18) Laermer, F.; Elsaesser, T.; Kaiser, W. Chem. Phys. Lett. **1988**, *148*, 119.
(19) Wiechmann, M.; Port, H. *J. Lumin.* **1991**, *48/49*, 217.
(20) Wiechmann, M.; Port, H.; Frey, W.; Laermer, F.; Elsaesser, T. *J. Phys. Chem.* **1991**, *95*, 1918.
(21) Wiechmann, M.; Port, H.; Laermer, F.; Frey, W.; Elsaesser, T. *Chem. Phys. Lett.* **1990**, *165*, 28.
(22) Chudoba, C.; Lutgen, S.; Jentzsch, T.; Riedle, E.; Woerner, M.; Elsaesser, T. *Chem. Phys. Lett*. **1995**, *240*, 35.
(23) Chudoba, C.; Riedle, E.; Pfeiffer, M.; Elsaesser, T. *Chem. Phys. Lett*. **1996**, *263*, 622.
(24) Lochbrunner, S.; Wurzer, A. J.; Riedle, E. *J. Chem. Phys*. **2000**, *112*, 10699.
(25) Lochbrunner, S.; Schultz, T.; Schmitt, M.; Shaffer, J. P.; Zgierski, M. Z.; Stolow, A. *J. Chem. Phys*. **2001**, *114*, 2519.
(26) Lochbrunner, S.; Stock, K.; De Waele, V.; Riedle, E. In *Femtochemistry and Femtobiology: Ultrafast Dynamics in Molecular Science*; Douhal, A., Santamaria, J., Eds.; World Scientific: River Edge, NJ, 2002; p 202.
(27) Stock, K.; Bizjak, T.; Lochbrunner, S. *Chem. Phys. Lett*. **2002**, *354*, 409.
(28) Sekikawa, T.; Kobayashi, T.; Inabe, T. *J. Phys. Chem. B* **1997**, *101*, 10645.
(29) Jethwa, J.; Ouw, D.; Winkler, K.; Hartmann, N.; Vöhringer, P. *Z. Phys. Chem*. **2000**, *214*, 1367.
(30) Fournier, T.; Pommeret, S.; Mialocq, J.-C.; Deflandre, A.; Rozot, R. *Chem. Phys. Lett*. **2000**, *325*, 171.
(31) Neuwahl, F. V. R.; Foggi, P.; Brown, R. G. *Chem. Phys. Lett*. **2000**, *319*, 157.
(32) Neuwahl, F. V. R.; Bussotti, L.; Righini, R.; Buntinx, G. *Phys. Chem. Chem. Phys.* **2001**, *3*, 1277.
(33) Sobolewski, A. L.; Domcke, W. In *The Reaction Path in Chemistry: Current Approaches and Perspectives*; Heidrich, D., Ed.; Kluwer Academic Publishers: Dordrecht, The Netherlands, 1995; p 257.
(34) Sobolewski, A. L.; Adamowicz, L. *Chem. Phys.* **1995**, *193*, 67.
(35) Sobolewski, A. L.; Domcke, W. *Chem. Phys*. **1994**, *184*, 115.
(36) Sobolewski, A. L.; Domcke, W. *Phys. Chem. Chem. Phys*. **1999**, *1*, 3065.
(37) Sobolewski, A. L.; Domcke, W. *J. Phys. Chem. A* **1999**, *103*, 4494.
(38) Sobolewski, A. L.; Domcke, W. *Chem. Phys. Lett*. **1999**, *300*, 533.
(39) Pfeiffer, M.; Lau, A.; Lenz, K.; Elsaesser, T. *Chem. Phys. Lett*. **1997**, *268*, 258.
(40) Pfeiffer, M.; Lenz, K.; Lau, A.; Elsaesser, T.; Steinke, T. *J. Raman Spectrosc*. **1997**, *28*, 61.
(41) Pfeiffer, M.; Lenz, K.; Lau, A.; Elsaesser, T. *J. Raman Spectrosc*. **1995**, *26*, 607.
(42) Marzocchi, M. P.; Mantini, A. R.; Casu, M.; Smulevich, G. *J. Chem. Phys*. **1998**, *108*, 534.
(43) Rini, M.; Kummrow, A.; Dreyer, J.; Nibbering, E. T. J.; Elsaesser, T. *Faraday Discuss*. **2002**, *122*, 27.
(44) Lochbrunner, S.; Wurzer, A. J.; Riedle, E. *J. Phys. Chem. A* **2003**, *107*, 10580.
(45) Rios, M. A.; Rios, M. C. *J. Phys. Chem. A* **1998**, *102*, 1560.
(46) Scheiner, S. *J. Phys. Chem. A* **2000**, *104*, 5898.
(47) Rios, M. A.; Rios, M. C. *J. Phys. Chem*. **1995**, *99*, 12456.
(48) Kar, T.; Scheiner, S.; Cuma, M. *J. Chem. Phys.* **1999**, *111*, 849.
(49) Frisch, M. J.; Trucks, G. W.; Schlegel, H. B.; Scuseria, G. E.; Robb, M. A.; Cheeseman, J. R.; Zakrzewski, V. G.; Montgomery, J. A., Jr.; Stratmann, R. E.; Burant, J. C.; Dapprich, S.; Millam, J. M.; Daniels, A. D.; Kudin, K. N.; Strain, M. C.; Farkas, O.; Tomasi, J.; Barone, V.; Cossi, M.; Cammi, R.; Mennucci, B.; Pomelli, C.; Adamo, C.; Clifford, S.; Ochterski, J.; Petersson, G. A.; Ayala, P. Y.; Cui, Q.; Morokuma, K.; Malick, D. K.; Rabuck, A. D.; Raghavachari, K.; Foresman, J. B.; Cioslowski, J.; Ortiz, J. V.; Stefanov, B. B.; Liu, G.; Liashenko, A.; Piskorz, P.; Komaromi, I.; Gomperts, R.; Martin, R. L.; Fox, D. J.; Keith, T.; Al-Laham, M. A.; Peng, C. Y.; Nanayakkara, A.; Gonzalez, C.; Challacombe, M.; Gill, P. M. W.; Johnson, B. G.; Chen, W.; Wong, M. W.; Andres, J. L.; Head-Gordon, M.; Replogle, E. S.; Pople, J. A. *Gaussian 98*; Gaussian, Inc.: Pittsburgh, PA, 1998.
(50) Allouche, A. *Spectrochim. Acta* **1993**, *49A*, 571.
(51) Kurtz, L.; Hofmann, A.; de Vivie-Riedle, R. *J. Chem. Phys*. **2001**, *114*, 6151.
(52) Nickel, B.; Walla, P. J. *Chem. Phys.* **1998**, *237*, 371.
(53) Fores, M.; Duran, M.; Sola, M. *Chem. Phys*. **2000**, *260*, 53.
(54) Catalán, J.; Palomar, J.; de Paz, J. L. G. *J. Phys. Chem. A* **1997**, *101*, 7914.
(55) Hofmann, A.; de Vivie-Riedle, R. *J. Chem. Phys*. **2000**, *112*, 5054.
(56) De Waele, V.; Buntinx, G.; Poizat, O.; Flament, J.-P.; Kassab, E. *J. Chem. Phys*. **1999**, *110*, 6353.
(57) De Waele, V.; Buntinx, G.; Poizat, O.; Flament, J.-P. *J. Raman Spectrosc*. **2000**, *31*, 275.
(58) Guallar, V.; Batista, V. S.; Miller, W. H. *J. Chem. Phys*. **2000**, *113*, 9510.
(59) Kiefer, P. M.; Hynes, J. T. *J. Phys. Chem. A* **2002**, *106*, 1834.
(60) Kiefer, P. M.; Hynes, J. T. *J. Phys. Chem. A* **2002**, *106*, 1850.
(61) Naundorf, H.; Worth, G. A.; Meyer, H.-D.; Kühn, O. *J. Phys. Chem. A* **2002**, *106*, 719.
(62) Madsen, D.; Stenger, J.; Dreyer, J.; Nibbering, E. T. J.; Hamm, P.; Elsaesser, T. *Chem. Phys. Lett*. **2001,** *341*, 56.
(63) Weiss, J.; May, V.; Ernsting, N. P.; Farztdinov, V.; Mühlpfordt, A. *Chem. Phys. Lett*. **2001**, *346*, 503.
(64) Batista, V. S.; Brumer, P. *Phys. Rev. Lett*. **2002**, *89*, 143201.